applied sciences

MDPI

Article

A Novel Method for Automatically and Accurately Diagnosing Demagnetization Fault in Direct-Drive PMSMs Using Three PNNs

Yiyong Xiong, Jinghong Zhao, Sinian Yan, Kun Wei * and Haiwen Zhou *

School of Electrical Engineering, Naval University of Engineering, Wuhan 430030, China; xiongyiyong1989@163.com (Y.X.); zhaojinghong@163.com (J.Z.); ysnian0504@126.com (S.Y.)
* Correspondence: wei.kunn@aliyun.com (K.W.); littlesimon90@163.com (H.Z.)

Abstract: Direct-drive permanent magnet synchronous machines (DDPMSMs) have recently become an ideal candidate for applications such as military, robotics, electric vehicles, etc. These machines eliminate the need for a transmission mechanism and excitation coil circuits, which enhances the system's overall efficiency and decreases the likelihood of failures. However, it may incur demagnetization faults. Due to the characteristic of having a large number of pole pairs, this type of machine exhibits numerous demagnetization fault modes, which poses a challenge in locating demagnetization faults. This paper proposed a probabilistic neural network (PNN)-based diagnostic system to detect and locate demagnetization faults in DDPMSMs, using information obtained through three toroidal-yoke-type search coils arranged at the bottom of the stator slot. A rotor partition method is proposed to solve the problem of demagnetization fault location difficulty caused by various fault modes. Demagnetization fault location is achieved by sequentially diagnosing the condition of each partition of permanent magnets. Three demagnetization fault identified signals (DFISs) are constructed by the voltage of the three toroidal-yoke coils, which are used as inputs of PNNs. Three PNNs have been designed to map the extracted features and their corresponding types of demagnetization faults. The database for training and testing the PNNs is generated from a DDPMSM with different demagnetization conditions and different operating conditions, which are established through an experimentally validated mathematical model, an FEM model, and experiments. The simulation and experimental test results showed that the accuracy in diagnosing the location of the demagnetization fault is 99.2% when the demagnetization severity is 10%, which demonstrates the effectiveness of the proposed three PNN-based diagnostic approach.

Keywords: demagnetization fault; fault detection; fault localization; permanent magnet synchronous machine (DDPMSM); probabilistic neural network (PNN); toroidal-yoke-search coil

check for updates

Citation: Xiong, Y.; Zhao, J.; Yan, S.; Wei, K.; Zhou, H. A Novel Method for Automatically and Accurately Diagnosing Demagnetization Fault in Direct-Drive PMSMs Using Three PNNs. *Appl. Sci.* **2024**, *14*, 11943. https://doi.org/10.3390/app142411943

Academic Editor: Pedro Couto

Received: 15 November 2024
Revised: 17 December 2024
Accepted: 17 December 2024
Published: 20 December 2024

Copyright: © 2024 by the authors. Licensee MDPI, Basel, Switzerland. This article is an open access article distributed under the terms and conditions of the Creative Commons Attribution (CC BY) license (https://creativecommons.org/licenses/by/4.0/).

1. Introduction

To meet the requirements for applications such as electric vehicles and robotics, electric machines should possess certain characteristics: compact structure, high reliability, and high safety. The direct-drive permanent magnet synchronous machine (DDPMSM) has gained increasing popularity in these fields due to its advantages, including high efficiency, high torque density, and high power density [1–3]. However, the DDPMSM is subject to demagnetization faults, owing to factors such as a high operating temperature, the armature reaction, the aging of permanent magnet (PM), and manufacturing defects [4]. Additionally, DDPMSMs used for offshore platform power generation and marine propulsion face increased risks of demagnetization, as the presence of seawater significantly heightens the likelihood of NdFeB magnets losing their magnetism. This fault will lead to the poor performance of the machine, and even complete failure of the machine and its drive system if not detected early and eliminated. Moreover, it causes massive economic losses and disastrous outcomes [5]. The early detection and location of demagnetization faults in

PMSMs will help to prevent serious failures, reduce maintenance time and costs, and prevent unscheduled downtime [6]. Hence, having an automatic demagnetization fault location system is very important and increases the reliability, availability, and safety of PMSMs, and more importantly, is the basis of fault tolerance and maintenance.

Several research studies have been conducted to diagnose demagnetization faults in PMSMs. Most of the methods are based on a spectrum analysis of stator current [7,8], stator voltage [9], vibration and noise [10], etc. Motor current signature analysis (MCSA) is the most popular and common diagnosis approach for a demagnetization fault. This method does not require extra equipment for measuring current and is noninvasive. However, the MCSA-based demagnetization fault diagnosis method has some limitations in that diagnosis accuracy and sensitivity are easily affected by operating conditions and controller parameters [7,8,11]. To overcome the issues of the MCSA-based method influenced by the inverter and controller regulator, a zero-sequence voltage component (ZSVC)-based method has been developed to diagnose the demagnetization fault. This method requires an accessible neutral point of the stator windings, resistor network, and voltage sensor to measure the ZSVC [9,12]. When a PMSM incurs a demagnetization fault, its torque and speed will ripple, resulting in vibration and noise. Harmonic components of specific frequencies extracted from the measured vibrations or noise by fast Fourier analysis (FFT) or time-frequency analysis are applied for partial demagnetization fault detection [10]. Vibration and noise signals are often affected by environmental noise and other interference signals in practical applications, which may lead to inaccurate analysis results. Furthermore, apart from the abovementioned limitations, the fault signature characteristics of the spectrum analysis-based methods depend on the number of poles and slots, stator winding configuration, and the number, location, and severity of demagnetized permanent magnets; therefore, it is not easy to generalize this approach for various PMSMs. In addition, the spectrum analysis-based methods can detect a partial demagnetization fault, but cannot detect a uniform demagnetization fault. Another limitation of the above methods is the ineffectiveness of detecting the location of demagnetized permanent magnets because the signals utilized are obtained from outside the machine.

Demagnetization faults in PMSMs cause changes in the stator magnetic field, which are directly reflected in the induced voltage of the search coil installed in the stator. Therefore, both the stator magnetic field and the induced voltage of the search coil contain rich demagnetization fault information, such as the number and position of demagnetized permanent magnets, which makes demagnetization fault diagnosis methods based on magnetic signals increasingly popular [13,14]. Therefore, the magnetic signal-based methods for detecting the occurrence and location of demagnetization faults are the mainstream methods. Additional search coils have been used to measure the magnetic flux or back EMF for the online diagnosis of demagnetization faults in PMSMs. In [15], search coils are wound around each stator tooth in the machine to measure stator tooth magnetic flux, and the fault indicators extracted from tooth magnetic flux are used to diagnose demagnetization faults. Nonetheless, this approach can only diagnose the number of demagnetized permanent magnets. In [16], twelve search coils are installed on each stator tooth in PMSM. The fundamental components of the induced voltages from these search coils are utilized to monitor machine health condition and to detect various faults, such as eccentricity faults, interturn short-circuit faults (ISCF), and demagnetization faults. The location of demagnetized permanent magnets can be accurately identified by using a polar graph of the decoupled field components of the voltages of all search coils. This method allows for a precise assessment of the permanent magnet's condition in a PMSM with a single demagnetized permanent magnet. The current search coil-based diagnostic methods for demagnetization faults have limitations regarding invasiveness, size, and installation [11,15,16]. Hence, this method is not suitable for DDPMSMs with a high number of poles. Furthermore, the characteristic values of the voltage signal from the search coil are influenced by the saturation level of the stator teeth. The comparison of the demagnetization fault diagnosis methods mentioned above is listed in Table 1.

Table 1. Comparison of demagnetization fault diagnosis methods.

References	Methods	Advantages	Limitations
[7,8,11]	MCSA-based method	non-invasive, online	sensitivity to operating conditions, controller parameters, and poor sensitivity
[9,12]	ZSVC-based method	non-invasive, online, more sensitive performance than the MCSA-based method	requires an accessible neutral point for the stator windings, resistor network, and voltage sensor to measure the ZSVC
[10]	Vibration/noise signal-based method	non-invasive, online, low cost	affected by environmental noise and other interference signals
[11–16]	Search coil-based method	more sensitive than above two methods, online, can locate demagnetized magnets	highly invasive, causing complex manufacturing processes for PMSMs, can locate demagnetized magnets in a PMSM with a single demagnetized permanent magnet

To address the limitations of current methods, a novel approach based on toroidal-yoke-search coils is proposed in this paper to accurately diagnose demagnetization faults for DDPMSMs with a high number of poles; it is also applicable to any PMSM. This novel method involves installing three toroidal-yoke-search coils at the bottom of the stator slot to measure the magnetic flux in the stator yoke. Despite the requirement of installing additional search coils, it effectively captures sensitive characteristics of demagnetization faults and is largely unaffected by magnetic circuit saturation, and the number of search coils in this method is greatly reduced. Moreover, this low-cost built-in sensor can detect at the initial stage of the occurrence of partial and uniform demagnetization in DDPMSMs. To tackle the issue of difficulty in locating demagnetized permanent magnets caused by the multiple types of demagnetization faults in DDPMSM, firstly the rotor is divided into p modules (p is the number of pole pairs of machines), with each module consisting of a pair of permanent magnets, and then the condition of each pair of permanent magnets is diagnosed in sequence, and finally, the location of the demagnetized permanent magnets can be identified. Toroidal-yoke-search coils are wound around the stator yoke, located inside and outside the bottom of the stator slot. The distance between adjacent toroidal-yoke-search coils is equal to or close to one pole distance. It is also shown that this method is independent of motor topology and winding configurations, and it is easy to generalize the method for various PMSMs.

Due to machine systems in fields like aerospace, military, marine propulsion, and robotics becoming increasingly complex and expensive, the demand for precise and automated fault diagnosis systems is rising. Accordingly, artificial intelligence tools have been introduced in fault diagnosis to enhance automation and accuracy, such as the support vector machine (SVM) [17], K-Nearest Neighbor (KNN) [18], and artificial neural networks (ANNs) [19,20]. In [17], two different SVM models were trained to detect faulty phases for stator-windings turn faults and ground faults. The SVM algorithm can solve machine learning problems with small samples and has good generalization ability. However, it has some limitations, such as a long training time, difficulty in determining model parameters, and the need for multiple models to be constructed to deal with multi-classification problems. For multilabel classification problems, the KNN algorithm is utilized. In [18], a KNN model is designed with an eight-dimensional feature vector and fourteen fault type labels to classify various faults. However, it also has the drawback of difficulty in determining model parameters and high computational complexity. The ANN is very attractive in the field of fault classification; it has gained popularity over other tools thanks to its enormous advantages, such as strong nonlinear mapping ability, very short execution

times, and strong generalization capability [19–21]. In [19], a feed-forward multilayer perception artificial neural network (MLP-ANN) is used to distinguish current fluctuations caused by short-circuit faults from those caused by load changes. In [20], a feed-forward MLP-ANN is utilized to automatically identify the faulty phase in the event of ISCF faults and phase-to-phase faults. In [21], an ANN-based diagnostic tool is developed to detect the location and severity of ISCF in line-start PMSMs. However, to achieve optimal performance of the ANN-based fault diagnosis method, various neural network structures with different numbers of hidden layers and neurons should be trained. It is shown that the design process of the ANN-based diagnosis model is complex. The PNN is widely used in pattern recognition and fault diagnosis due to the advantages of the easy and fast training of the network and no requirement for a large number [22,23]. The comparison of artificial intelligence-based fault diagnosis methods for PMSMs mentioned above is listed in Table 2.

Table 2. Comparison of artificial intelligence-based fault diagnosis methods for PMSMs.

References	Methods	Advantages	Limitations
[17]	SVM-based method	effective for small sample data, strong generalization ability	low training efficiency for large-scale data, multiclassification problems are complex to handle, difficulties in kernel function selection and parameter adjustment
[18]	KNN-based method	no training process (non-parametric model), able to handle complex data distributions	high computational complexity, sensitive to the curse of the dimensionality of data, sensitive to the distribution and proportion of data
[19–21]	ANN-based method	strong learning ability, parallel processing capabilities, and a certain tolerance for noise and partially missing data in the data	requires a large amount of data and computing resources, prone to overfitting, difficulties in network structure and parameter selection
[22,23]	PNN-based method	learning process is simple, high classification accuracy, insensitive to outliers	need to determine the smoothing coefficient

According to the above analysis, a three probabilistic neural networks (PNNs)-based fault diagnosis system was developed to automatically and accurately detect demagnetization faults and identified the demagnetized permanent magnets in DDPMSMs using the signals from three toroidal-yoke-search coils. Considering the influence of operating conditions and demagnetization fault parameters, three demagnetization faults identified signals (DFISs) were constructed by the voltage of the three toroidal-yoke-search coils. The DFISs are directly input to PNNs, then the PNNs extract fault features and classify fault modes. This method can not only reduce the dependence on artificial feature engineering, but also reduce the computational requirements.

The rest of the paper is organized as follows. Section 2 will introduce the construction, modeling, and analysis of DFIS for accurately diagnosing demagnetization fault. Section 3 will develop an automatic and accurate demagnetization fault diagnosis system using three PNNs. In Section 4, multiple demagnetization fault cases from finite element simulation and experiments will be used to validate the correctness and effectiveness of the proposed demagnetization fault diagnosis method. Section 5 draws the conclusions.

2. Construction, Modeling, and Analysis of Fault Characteristic Signals for Diagnosing Demagnetization Faults

2.1. Construction of Demagnetization Fault Indications

2.1.1. Placement of Toroidal-Yoke-Search Coil

The placement of sensors to obtain fault signatures is the most significant step in the fault diagnosis architecture. The placement of the search coil for obtaining the demagnetization fault information is shown in Figure 1. Three additional toroidal-yoke coils (TYC1, TYC2, and TYC3) are wound around the stator yoke to measure the stator yoke flux at

different positions of the stator, and the distance between adjacent toroidal-yoke coils is approximately polar distance to strengthen fault demagnetization characteristics.

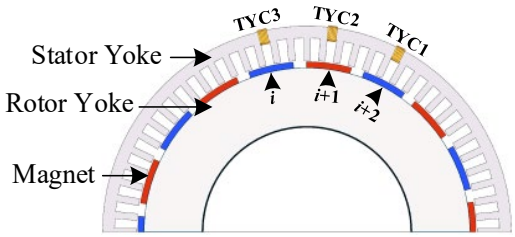


Figure 1. Placement scheme of toroidal-yoke-search coil.

2.1.2. Building of Demagnetization Fault Identified Signal

The selection of the demagnetization fault identified signal (DFIS) sets the stage for an efficient and accurate demagnetization fault diagnosis. The DFIS should include sufficient information about the condition of permanent magnets to enable the detection and identification of demagnetization faults.

The voltages measured by the toroidal-yoke coils are the back EMF, which are induced by the stator yoke flux linking the search coil. The voltage signals obtained from three toroidal-yoke coils cannot be directly utilized for the detection of demagnetization faults and the identification of demagnetization fault modes, and must be further processed to achieve the DFIS.

Based on the voltage signals measured by three toroidal-yoke coils, three DFISs are constructed to identify the occurrence and mode of demagnetization faults, thereby achieving the localization of demagnetized permanent magnets. The main identification signal (SI_m) is obtained by subtracting the residual voltage in TYC1 from TYC2 (residual voltage is the difference between the measured voltage and the voltage under the healthy condition of the machine); the first auxiliary identification signal (SI_{a1}) is obtained by subtracting the residual voltage in TYC1 from TYC3; and the second auxiliary identification signal (SI_{a2}) is obtained by subtracting the residual voltage in TYC2 from TYC3.

2.2. Modeling of Demagnetization Fault Identified Signal

In order to analyze the effect of the number, location, and severity of demagnetized permanent magnets on the DFISs, the partitioned mathematical model in [13] is adopted to analyze DFISs under healthy and different demagnetization fault modes.

2.2.1. Modeling of the Main Identification Signal

The main identification signal $SI_{\text{m-PM}k}$ generated by the kth PM (PMk, k is the PM number, which is the natural number ranging from 1 to 2p) is expressed as in (1).

$$\begin{cases} SI_{\text{m-PM}k} = (-1)^{k-1} E_1 \sin(\alpha - (k-1)\pi) \\ (k-1)\pi \le \alpha \le (k+1)\pi \end{cases}, \quad (1)$$

where E_1 is the amplitude of the fundamental component of $SI_{\text{m-PM}k}$. α represents the electrical angle between a point on the inner circle of the stator and the origin of the coordinates. The coordinate origin is defined as the intersection point of the coil axes and the inner circle of the stator. The coil axes refer to the axes of TYC1 and TYC2. When the axes of PM1 and PM2 align with the coil axes of TYC1 and TYC2 for the first time, the search coil begins to collect signals.

The ith electrical period signal of SI_m ($SI_{\text{m-}i}$) can be derived as follows:

$$SI_{\text{m-}i} = \begin{cases} SI_{\text{m-PM(2p)}} + SI_{\text{m-PM1}} + SI_{\text{m-PM2}} \quad (i = 1) \\ \sum_{k=2i-2}^{2i} SI_{\text{m-PM}k} \quad (i = 2, 3, 4 \ldots\ldots p) \end{cases}, \quad (2)$$

where i represents the number of pole pairs, as well as representing the number of electric cycles of the identification signal, and i has a value from 1 to p. Taking $i = 1$ as an example, 1 represents the first pair of magnets and the first electrical cycle signal of SI_{m}.

2.2.2. Modeling of the First Auxiliary Identification Signal

The first auxiliary identification signal $SI_{\text{a1-PM}k}$ generated by the PMk is calculated through (3).

$$SI_{\text{a1-PM}k} = \begin{cases} |E_1 \sin(\alpha - (k-1)\pi)| & (k-1)\pi \le \alpha \le k\pi \\ 0 & k\pi \le \alpha \le (k+1)\pi \\ |E_1 \sin(\alpha - (k-2)\pi)| & (k+1)\pi \le \alpha \le (k+2)\pi \end{cases}, \tag{3}$$

The ith electrical period signal of SI_{a1} ($SI_{\text{a1-}i}$) is described in

$$SI_{\text{a1-}i} = \begin{cases} \sum_{k=2p-1}^{2p} SI_{\text{a1-PM}k} + \sum_{k=1}^{2} SI_{\text{a1-PM}k} & (i = 1) \\ \sum_{k=2i-3}^{2i} SI_{\text{a1-PM}k} & (k = 2, 3, 4 \ldots\ldots p) \end{cases}, \tag{4}$$

2.2.3. Modeling of the Second Auxiliary Identification Signal

The second auxiliary identification signal $SI_{\text{a2-PM}k}$ generated by the PMk is calculated through (5).

$$\begin{cases} SI_{\text{a2-PM}k} = (-1)^{k-1} E_1 \sin(\alpha - k\pi) \\ k\pi \le \alpha \le (k+2)\pi \end{cases}, \tag{5}$$

The ith electrical period signal of SI_{a1} ($SI_{\text{a1-}i}$) is calculated through Equation (6).

$$SI_{\text{a2-}i} = \begin{cases} SI_{\text{a2-PM(2p-1)}} + SI_{\text{a2-PM(2p)}} + SI_{\text{a2-PM1}} & (i = 1) \\ \sum_{k=2i-3}^{2i-1} SI_{\text{a1-PM}k} & (i = 2, 3, 4 \ldots\ldots p) \end{cases}, \tag{6}$$

The effectiveness and accuracy of the partitioned mathematical model of the main identification signal, the first auxiliary identification signal, and the second auxiliary identification signal are validated in [13].

2.3. Analysis of Demagnetization Fault Identified Signal

2.3.1. Analysis of the Main Identification Signal

According to (2), each electrical period waveform of SI_{m} depends on the healthy conditions of three permanent magnets coupled to TYC1 and TYC2. Each permanent magnet has two fundamental conditions: a healthy condition and a demagnetized condition. This study uses a binary coding approach to effectively represent these conditions, where the healthy condition is denoted by 0 and the demagnetized condition is represented by 1. To comprehensively indicate the states of three permanent magnets, a three-bit binary number is employed, with each bit corresponding to the condition of one magnet. Accordingly, all possible combinations of these three permanent magnets can be encoded into eight distinct fault modes, represented by binary sequences ranging from 000 to 111, which are listed in Table 3. Each binary sequence accurately maps to a specific combination of conditions for the permanent magnets. In this section, the electrical period waveform of SI_{m} under eight distinct demagnetization fault modes will be analyzed.

In Table 3, a value of 0 indicates that the corresponding numbered permanent magnet is in healthy condition, and a value of 1 signifies that the corresponding numbered permanent magnet is in demagnetized condition. i indicates the electric cycle number of SI_{m}; $2i - 2$, $2i - 1$, and $2i$ represent the permanent magnet number. Take Mode 2 in Table 3 as an example to illustrate the relationship between characteristics of SI_{m}, permanent

magnet status, and demagnetization fault modes. When the SI_m has a signal in the first electric cycle ($i = 1$), Mode 2 (001) indicates that PM($2p$) and PM1 are healthy, and PM2 is demagnetized. When SI_m has a signal in the ith electric cycle ($i \geq 2$), Mode 2 indicates that PM($2i - 2$) and PM($2i - 1$) are healthy, and PM($2i$) is demagnetized.

Table 3. Demagnetization fault modes code.

Demagnetization Fault Mode	PM Number or Electrical Period Number ($i = 1$)			PM Number or Electrical Period Number ($1 < i \leq p$)		
	$2p$	1	2	$2(i-1)$	$2i-1$	$2i$
Mode 1(000)	0	0	0	0	0	0
Mode 2(001)	0	0	1	0	0	1
Mode 3(110)	1	1	0	1	1	0
Mode 4(011)	0	1	1	0	1	1
Mode 5(100)	1	0	0	1	0	0
Mode 6(010)	0	1	0	0	1	0
Mode 7(101)	1	0	1	1	0	1
Mode 8(111)	1	1	1	1	1	1

In order to elaborate and analyze the effect of different permanent magnet numbers, locations, and severities on the DFISs, a three-phase surface-mounted DDPMSM with forty-eight-slots/forty-four-poles is employed. The specifications of this machine are presented in Table 4. These parameters are also those of the machine used to establish the samples database in Section 4, as well as the experimental test machine of the machine fault characteristic test platform in Section 5.

Table 4. The key specifications of the test DDPMSM.

Items	Values	Unit
Rated power	1.5	kW
Rated current	4	Arms
Rated speed	180	rpm
Rated frequency	66	Hz
Number of phases	3	/
Number of parallel circuits per phase	1	/
Number of coils	24	/
Air-gap length	0.9	mm
Stator out diameter	270	mm
Stator inner diameter	203	mm
Permanent magnet thickness	4.5	mm
Permanent magnet width	11	mm
Permanent magnet length	100	mm
Permanent magnet material	NdFeB	/
Pole-arc coefficient	0.73	/
Slot–pole combination	48-slot/44-pole	/

Take the second electrical cycle signal of SI_m ($SI_{m\text{-}2}$) as an example to analyze the waveform characteristics corresponding to each demagnetization fault mode. According to Table 3, $SI_{m\text{-}2}$ relies on the healthy conditions of PM2, PM3, and PM4, which correspond to eight fault mode codes ranging from Mode (000) to Mode (111). The established mathematical model in Section 2.2 is used to analyze the $SI_{m\text{-}2}$ of the test machine under the eight demagnetization fault modes (the demagnetization severity of a single permanent magnet is 0.5); the results are shown in Figure 2.

As shown in Figure 2a, the second electrical cycle waveforms of SI_m ($SI_{m\text{-}2}$) under Mode 1 to Mode 6 are different from each other. Moreover, the $SI_{m\text{-}2}$ waveform trends of these six fault modes are different, so their identification is not affected by demagnetization

severity. Therefore, the $SI_{m\text{-}2}$ can discriminate six fault modes including Mode 1 to Mode 6, and then, determine the healthy condition of PM2, PM3, and PM4.

As shown in Figure 2b, the waveform trends of $SI_{m\text{-}2}$ under the three fault modes including Mode 6, Mode 7, and Mode 8 are the same, but the amplitudes are different. The amplitude of $SI_{m\text{-}2}$ depends on demagnetization severity. Hence, in the following discussion, the effect of demagnetization severity on $SI_{m\text{-}2}$ is investigated.

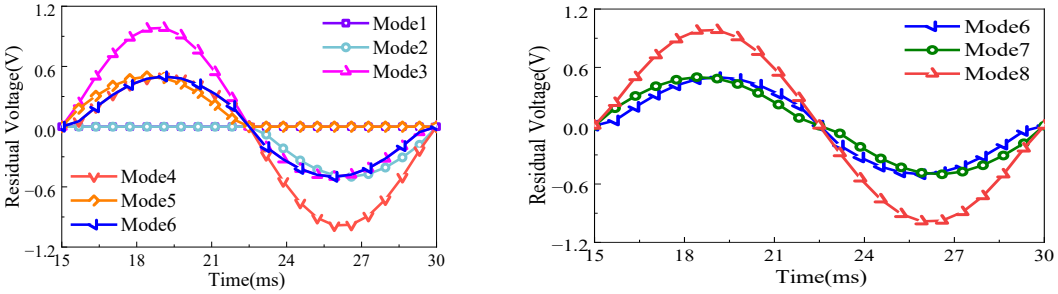


Figure 2. The waveforms of SI_{m-2}. (**a**) Mode 1 to 6. (**b**) Modes 6, 7, and 8.

2.3.2. Effect of Demagnetization Severity on SI_{m-2}

The waveforms of $SI_{m\text{-}2}$ of the employed DDPMSM under Mode 7 with 100% demagnetization and Mode 8 with 50% demagnetization, are studied and presented in Figure 3.

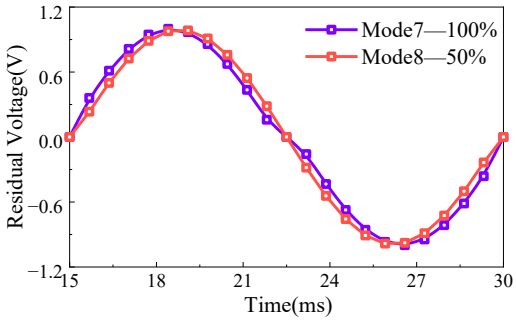


Figure 3. The waveforms of SI_{m-2} under Mode 7 with 100% demagnetization and Mode 8 with 50% demagnetization.

As shown in Figure 3, the waveforms of SI_{m-2} are the same for Mode 7 with 100% demagnetization and Mode 8 with 50% demagnetization. Therefore, Mode 7 and Mode 8 are identified to be the same fault mode. As shown in Figure 2b, the waveforms of $SI_{m\text{-}2}$ are different for Mode 7 with 50% demagnetization and Mode 8 with 50% demagnetization. Therefore, Mode 7 and Mode 8 are identified to be different fault modes. It can be noticed that, the waveforms of these two fault modes are sometimes the same and sometimes different, causing confusion when identifying them. This is due to the amplitude of $SI_{m\text{-}2}$ changing with the variation in the demagnetization severity, resulting in the waveforms for different fault modes with the same waveform trend sometimes being the same and sometimes being different. To solve the difficulty of demagnetization fault mode identification caused by demagnetization severity, SI_m is normalized through (7).

$$s_{norm} = \frac{s}{|s_{max}|}, \tag{7}$$

where S_{norm} is the normalized value. S is the actual value. S_{max} is the maximum value of one electrical cycle signal.

The normalized $SI_{m\text{-}2}$ under six different demagnetization fault modes, including Mode 6 with 100% demagnetization, Mode 6 with 50% demagnetization, Mode 7 with

100% demagnetization, Mode 7 with 50% demagnetization, Mode 8 with 100% demagnetization, and Mode 8 with 50% demagnetization, are shown in Figure 4.

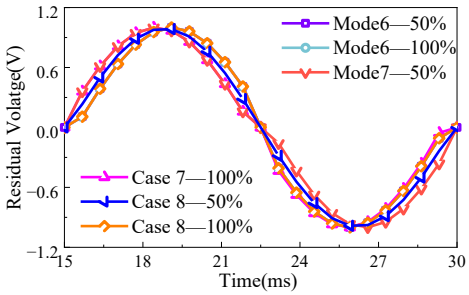


Figure 4. Normalized SI_{m} under six different demagnetization fault modes.

As shown in Figure 4, the waveforms of normalized SI_{m} are the same for these six different demagnetization fault modes. Thus, Mode 6, Mode 7, and Mode 8 are determined to be the same fault mode. Confusion caused by different demagnetization severities in the determination of the demagnetization fault modes can be eliminated by normalization. However, SI_{m} cannot discriminate between Mode 6, Mode 7, and Mode 8. To identify Mode 6, Mode 7, and Mode 8, the first auxiliary identification signal is applied.

2.3.3. Analysis of the First Auxiliary Identification Signal

According to (4), the first electrical cycle waveform of SI_{a1} ($\mathrm{SI_{a1\text{-}1}}$) relies on the healthy condition of PM1, PM2, PM(2p − 1), and PM(2p). The ith ($i \geq 2$) electrical cycle waveform of SI_{a1} ($SI_{\mathrm{a1}\text{-}i}$) relies on the healthy conditions of PM($2i - 3$), PM($2i - 2$), PM($2i - 1$), and PM($2i$). When PM($2i - 3$) (PM(2p − 1)) is in a healthy condition, Mode 6, Mode 7, and Mode 8 are defined as Mode 6H, Mode 7H, and Mode 8H, respectively. When PM($2k - 3$) (PM($2p - 1$)) is in a demagnetization condition, Mode 6, Mode 7, and Mode 8 are defined as Mode 6D, Mode 7D, and Mode 8D, respectively. Therefore, the SI_{a1} under six different demagnetization fault modes listed in Table 5 is investigated.

Table 5. Six fault modes corresponding to four consecutive PMs.

Demagnetization Fault Mode	PM Number or Electrical Period Number (i = 1)				PM Number or Electrical Period Number ($1 < i \leq p$)			
	$2p - 1$	$2p$	1	2	$2k - 3$	$2k - 2$	$2k - 1$	$2k$
Mode 6H(0010)	0	0	1	0	0	0	1	0
Mode 7H(0101)	0	1	0	1	0	1	0	1
Mode 8H(0111)	0	1	1	1	0	1	1	1
Mode 6D(1010)	1	0	1	0	1	0	1	0
Mode 7D(1101)	1	1	0	1	1	1	0	1
Mode 8D(1111)	1	1	1	1	1	1	1	1

Take the second electrical cycle signal of SI_{a1} ($SI_{\mathrm{a1\text{-}2}}$) as an example to analyze the waveform characteristics corresponding to Mode 6, Mode 7, and Mode 8. According to Table 5, $SI_{\mathrm{a1\text{-}2}}$ relies on the healthy condition of PM1, PM2, PM3, and PM4, which correspond to six fault mode codes given in Table 3. The $SI_{\mathrm{a1\text{-}2}}$ under six different fault modes is calculated through (4) and normalized through (7); the results are shown in Figure 5.

As shown in Figure 5a, the waveforms of normalized $SI_{\mathrm{a1\text{-}2}}$ under these modes (Mode 6H, Mode 7H, Mode 6D, Mode 8H, and Mode 8D) are different from each other. Therefore, the normalized $SI_{\mathrm{a1\text{-}2}}$ can discriminate these five fault modes including Mode 6H, Mode 7H, Mode 8H (Mode 7D), Mode 6D, and Mode 8D, and then, determine the healthy condition of PM1 to 4.

As shown in Figure 5b, the waveform of normalized $SI_{\mathrm{a1-2}}$ under Mode 7D is the same as the waveform under Mode 8H. Therefore, the $SI_{\mathrm{a1-2}}$ cannot discriminate be-

tween Mode 7D and Mode 8H. To identify Mode 7D and Mode 8H, the second auxiliary identification signal is applied.

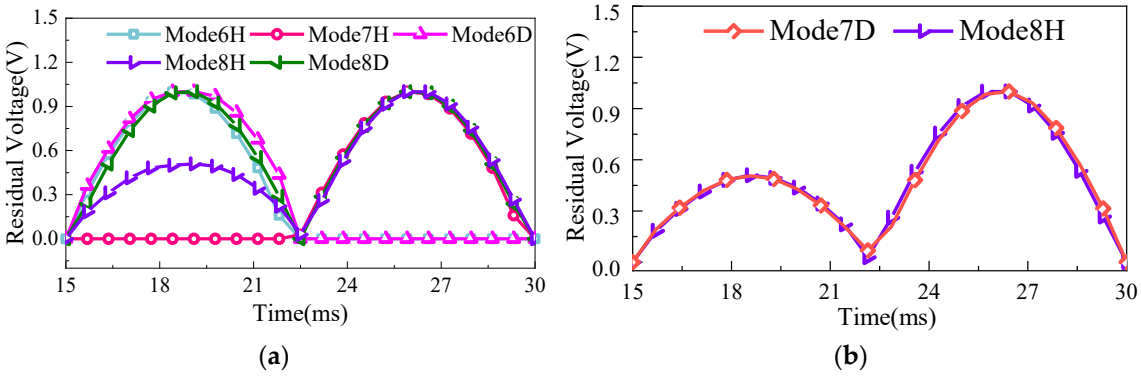


Figure 5. The waveforms of normalized $SI_{a1\text{-}2}$. (**a**) Mode 6H, Mode 7H, Mode 6D, Mode 8H, and Mode 8D. (**b**) Mode 7D and Mode 8H.

2.3.4. Analysis of the Second Auxiliary Identification Signal

Take the second electrical cycle signal of SI_{a2} ($SI_{a2\text{-}2}$) as an example to analyze the waveform characteristics corresponding to Mode 7D and Mode 8H. The $SI_{a1\text{-}2}$ under these two fault modes is calculated through (6) and normalized through (7); the results are shown in Figure 6.

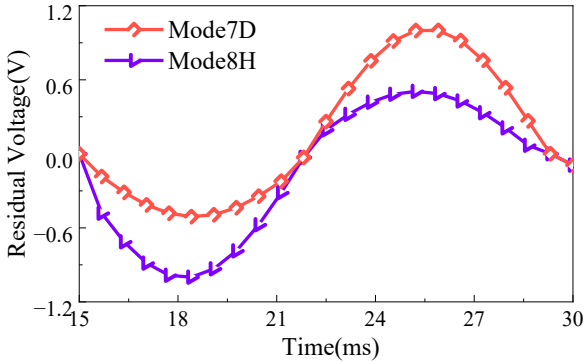


Figure 6. The waveforms of $SI_{a2\text{-}2}$ under Cas 7D or Mode 8H.

As shown in Figure 6, the waveform of normalized SI_{a2} under Mode 7D is different from the waveform under Mode 8H. Therefore, the SI_{a2} can identify Mode 7D and Mode 8H, and then, determine the healthy condition of PM1, PM2, PM3, and PM4.

According to the above analysis, two conclusions can be drawn.

(1) It can be clarified that by combining the signals SI_m, SI_{a1}, and SI_{a2}, any demagnetization fault mode can be accurately diagnosed, including uniform demagnetization and local demagnetization with different numbers, locations and severities. Modes 1 to 5 can be identified through SI_m. Mode 6H, Mode 6D, Mode 7H, and Mode 8D can be identified through SI_m and SI_{a1}. Mode 7D and Mode 8H can be identified through SI_m, SI_{a1}, and SI_{a2}.

(2) The healthy conditions of PM(2p), PM1, and PM2 can be accurately diagnosed through the first electrical cycle signal of DFISs. Thus, the healthy conditions of the first pair PM (PM1 and PM2) are identified through the first electrical cycle signal. The healthy conditions of PM2, PM3, and PM4 can be accurately diagnosed through the second electrical cycle signal of DFISs. The healthy condition of PM2 is already identified by the first electrical cycle signal, and thus, the healthy conditions of the second pair of PMs (PM3 and PM4) can be accurately diagnosed through the second electrical period signal. Accordingly, the healthy conditions of the ith-pair PMs (PM($2i-1$) and PM($2i$)) are identified through the ith electrical period signal of DFISs; the corresponding relationship between them is shown in Figure 7.

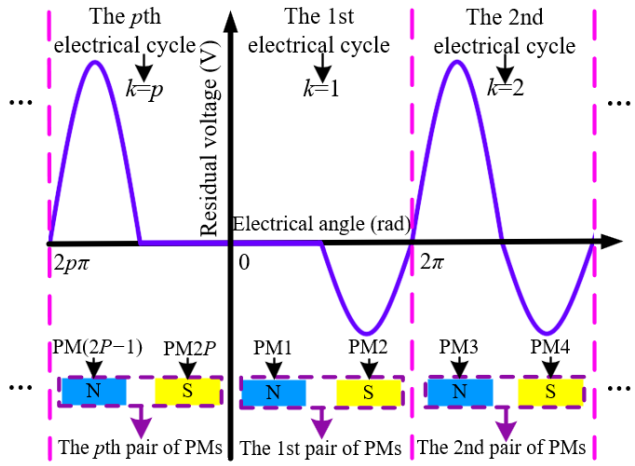


Figure 7. Corresponding relationship between the pole pair number and the electric cycle number of DFISs.

In summary, the proposed demagnetization fault diagnosis method is as follows: compare and analyze the actual measured waveform of the demagnetization fault identified signal with the various fault mode waveforms in Figures 4–6. When the measured waveform completely matches a certain fault mode waveform, it can be determined that the fault mode is the demagnetization fault mode of the corresponding permanent magnet pairs. Demagnetization faults in DDPSM can be accurately diagnosed by sequentially identifying the condition of each pair of permanent magnets. Thus, the healthy conditions of all of the permanent magnets can be determined through one complete rotation revolution.

2.4. Robustness of Demagnetization Fault Identified Signal

2.4.1. Effect of Load on Demagnetization Fault Identified Signal

The load of the machine is variable in actual applications. To diagnose the demagnetization faults under different loads, the fault identified signal needs to be robust to the load. This part is focused on the study and analysis of the demagnetization fault identified signal under different loading conditions (the speed of the test machine is rated speed, the demagnetization severity is 10%). Six different load conditions are studied, including no-load, 25% rated load, 50% rated load, 75% rated load, rated load, and 125% rated load. Take Mode 3 as an example to analyze the waveforms of SIm under different loading conditions, which are depicted in Figure 8.

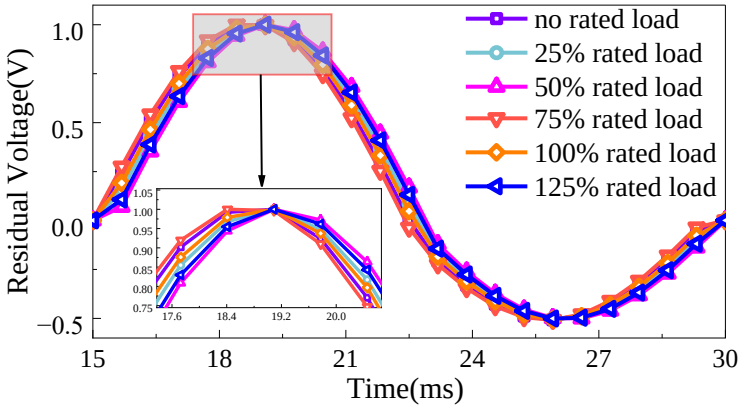


Figure 8. SI_m under different loading conditions of the machine.

As shown in Figure 8, even when the mode of demagnetization severity is 10%, SI_m are almost the same curve pattern under different loading levels, with small differences. Consequently, SI_m is almost insensitive to the variation in the loading conditions. The

behaviors of SI_{a1} and SI_{a2} are similar to SI_m. As a result, SI_m, SI_{a1}, and SI_{a2} are considered robust and discriminant signals to accurately diagnose demagnetization faults under different loading conditions.

2.4.2. Effect of Speed on Demagnetization Fault Identified Signal

The speed of machines is variable in actual applications. To diagnose the demagnetization faults under various speeds, the fault identified signal needs to be robust to the speed. This part is focused on the study and analysis of the demagnetization fault identified signal under various speeds (the load of the test machine is rated load, and the demagnetization severity is 10%). Two speed conditions are studied, including rated speed and 50% rated speed. Take Mode 3 as an example to analyze the waveforms of SI_m under different speed conditions, which are depicted in Figure 9.

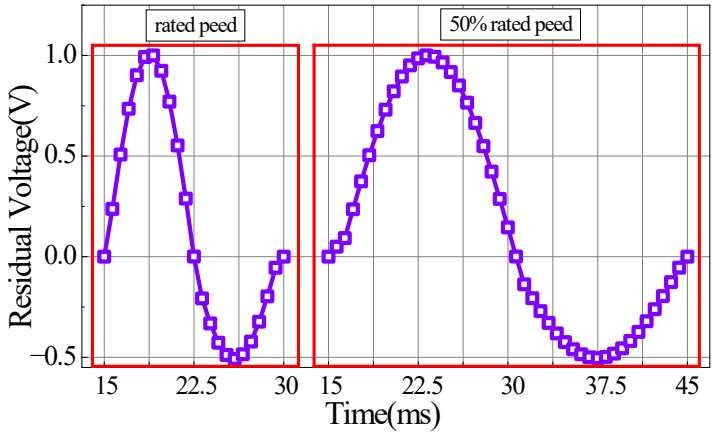


Figure 9. SI_m under various speeds of the machine.

As shown in Figure 9, even when the mode of demagnetization severity is 10%, the amplitudes of SI_m are almost the same for various speeds, with small differences. Consequently, SI_m is slightly affected by the variation in the machine speed. The behaviors of SI_{a1} and SI_{a2} are similar to SI_m. As a result, SI_m, SI_{a1}, and SI_{a2} are considered robust and discriminant characteristic signals to accurately locate demagnetization faults under various speeds.

3. Automatic Demagnetization Fault Diagnosis System Based on Three PNNs

3.1. The Process of Demagnetization Fault Diagnosis Using Three PNNs

The method for the automatic diagnosis of demagnetization faults in PMSMs using three PNNs is proposed, which can be roughly divided into a data collection and DFIS calculation module and a detection and location identification of fault module, as shown in Figure 10.

The specific steps of the proposed method are as follows:

(1) Measure the voltage of TYC1, TYC2, and TYC3.

(2) Calculate the residual voltage of TYC1, TYC2, and TYC3, and then, calculate SI_m, SI_{a1}, and SI_{a2}.

(3) If the peak value of SI_m is less than the set threshold (thd), the machine is healthy; otherwise, the machine is faulty.

(4) Partition SI_m, SI_{a1}, and SI_{a2} by electrical period.

(5) Input the first electric period signal of SI_m to the first PNN; then, the fault mode of the first pairs of permanent magnets is identified.

(6) If the output of the first PNN is not Mode 6 (Mode 6, Mode 7, and Mode 8 are identified as Mode 6), output the identified fault mode; otherwise, input the first electric period signal of SI_{a1} to the second PNN, and then the fault mode of the first pairs of permanent magnets is further identified.

(7) If the output of the second PNN is not Mode 8H or Mode 7D, output the identified fault mode; otherwise, input the first electric period signal of SI_{a2} to the second PNN, and then the fault mode of the first pairs of permanent magnets is finally identified.

(8) Determine the location of demagnetized permanent magnets in the first pairs of permanent magnets through the identified fault mode, Tables 3 and 5.

(9) Input the DFISs from the second electric cycle to the p-th electric cycle into the PNN in turn, and repeat steps 5 to 8 to diagnose the condition of each pair of permanent magnets. Determine the location of all demagnetized permanent magnets in the machine.

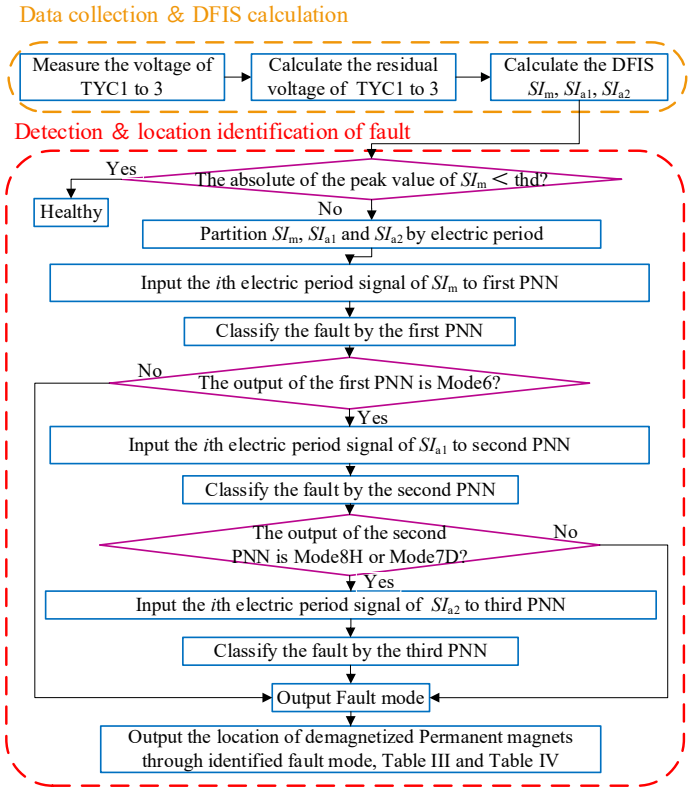


Figure 10. The process for automatically diagnosing demagnetization faults using three PNNs.

3.2. Design of the Automatic Demagnetization Fault Diagnosis System Using Three PNNs

3.2.1. Structure of the PNN

The PNN is widely used in pattern recognition and fault diagnosis due to, firstly, the training of the network being easy and fast [22,23]. Second, sparse samples are adequate for network performance. Third, it involves a single-pass network training stage without any iteration for adjusting weights. In addition, the PNN is easy to retrain with new data and adapts itself to architectural changes. Thus, the proposed system is based essentially on the use of three PNNs to achieve an automatic and intelligent demagnetization fault diagnosis system, which consists in automating the detection and the location of demagnetization faults in PMSMs. This section describes the design of the PNNs used as a tool for diagnosing the demagnetization faults in PMSMs.

The architecture of the PNN is shown in Figure 11, and is composed of four layers: an input layer, pattern layer, summation layer, and output layer. The input layer receives the signal from DFISs and further transfers the data to the pattern layer. The number of neurons in the input layer is one. The pattern layer calculates the relationships between the input feature vector and the demagnetization fault modes to be able to locate correctly the demagnetized PMs. The number of neurons in the pattern layer equals the size of training samples. The summation layer simply sums the outputs of the pattern layer neuron belonging to its own demagnetization fault mode. The output layer indicates automatically

the demagnetization fault mode corresponding to the fault presented at its inputs. The number of neurons in the output layer equal the number of demagnetization fault modes.

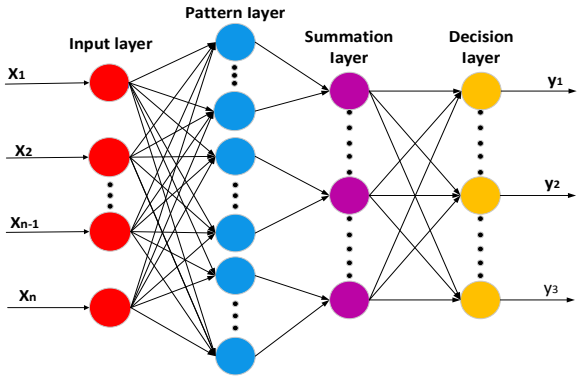


Figure 11. Architecture of the PNN.

3.2.2. The Design of Three PNNs

The first PNN consists in automating the detection and the discrimination of six demagnetization fault modes from Mode 1 to Mode 6. The input of the first PNN is SI_m. The first PNN is configured to have one output (O from 1 to 6), which is possible to indicate the mode of demagnetization fault. Therefore, six fault classes can be visualized. When the fault mode is Mode 1 to Mode 6, apply the same number as the demagnetization fault mode number to the output. When the fault mode is Mode 7 or Mode 8, apply 6 to the output. The output states of the first PNN are set to the following:

O=1 for Mode 1 (no fault);
O=2 for fault mode Mode 2;
⋮ ⋮
O=6 for fault mode Mode 6;
O=6 for fault mode Mode 7;
O=6 for fault mode Mode 8.

The second PNN consists in automating the discrimination of five demagnetization fault modes (Mode 6H, Mode 7H, Mode 8H (Mode 7D), Mode 6D, and Mode 8D). The input of the second PNN is S_{a1}. It is configured to have one output (O from 6 to 9), corresponding to the five demagnetization fault modes. The output states of the second PNN are set to the following:

O=6 for fault mode Mode 6H;
O=6 for fault mode Mode 6D;
O=7 for fault mode Mode 7H;
O=8 for fault mode Mode 8D;
O=9 for fault mode Mode 7D (Mode 8H).

The third PNN consists in automating the discrimination of two demagnetization fault modes (Mode 7D and Mode 8H). The input of the third PNN is S_{a2}. It has one output (O from 7 to 8), corresponding to the two demagnetization fault modes. The output states of the third PNN are set to the following:

O=7 for fault mode Mode 7D;
O=8 for fault mode is Mode 8H.

3.3. Database Creation

The PNNs have to learn the relationship between the DFISs presented as their inputs and corresponding demagnetization fault modes as their outputs. Thus, three specific and meaningful databases should be carefully prepared, which contain all possible demagnetization fault occurrences and even the healthy modes. The training data are obtained by simulation, using the demagnetization fault model proposed in Section 2 of this study as it is not possible to collect large faulty modes on a real machine.

The first database for training and testing the first PNN is composed of 132 examples of healthy modes and 924 examples of demagnetization faults of the employed PMSM, as shown in Table A1. A total of 1056 examples from the first database ($1 \times 22 \times 6 + 7 \times 22 \times 3 \times 2$) includes one healthy mode (Mode 1) and 22 electrical periods (1st~22nd) as well as 6 operating conditions (rated speed and no load, 25% rated speed and 25% rated load, 50% rated speed and 50% rated load, 75% rated speed and 75% rated load, rated speed and rated load, and 125% rated speed and 125% rated load), along with and seven demagnetization fault modes (Mode 2~Mode 8), 22 electrical periods (1st~22nd), 3 demagnetization severities (10%, 50%, 100%), and 2 operating conditions (rated speed and rated load, 50% rated speed, and 50% rated load). A total of 100 samples is randomly selected from the samples of each mode as training samples and the other 32 samples are selected as testing samples. Hence, the training database for the first PNN has 800 examples (8×100). To assess the generalization capacity of the adopted PNN, the testing data set should be different from the training data set. The testing database for the first PNN has 304 examples, including 256 examples (8×32) from the above 1056 examples and 48 examples with a different demagnetization severity from the training examples. The 48 examples ($1 \times 3 \times 2 + 7 \times 3 \times 2$) are composed of 6 examples of healthy mode (Mode 1) including 3 electrical periods and 2 operating conditions (50% rated speed and 25% rated load, and 75% rated speed and 50% rated load), along with seven demagnetization fault modes (Mode 2~Mode 8) including 3 electrical periods and 2 demagnetization severities (25% demagnetized (50% rated speed and rated load), and 75% demagnetized (rated speed and 50% rated load)).

The second database for training and testing the second PNN is composed of 840 examples, as shown in Table A2. A total of 792 examples of the second database ($6 \times 22 \times 3 \times 2$) includes 6 demagnetization fault modes (Mode 6H, Mode 7H, Mode 8H, Mode 6D, Mode 7D, and Mode 8D), 22 electrical periods (1st~22nd), and 3 demagnetization severities (10%, 50%, 100%) as well as 2 operating conditions (rated speed and rated load, 50% rated speed and 50% rated load). A total of 100 samples from each fault mode are randomly selected as training samples and the rest are selected as test samples. Hence, the training database for the second PNN has 600 examples. The testing database for the second PNN has 240 examples, including 192 examples from the above 792 examples and 48 examples with different demagnetization severities from the training examples. The 48 examples ($6 \times 4 \times 2$) are composed of 8 examples for each fault mode including 4 electrical periods and 2 demagnetization severities (25% demagnetized (50% rated speed and rated load), and 75% demagnetized (rated speed and 50% rated load)).

The third database for training and testing the third PNN is composed of 308 examples, as shown in Table A3. A total of 264 examples of the third database ($2 \times 22 \times 3 \times 2$) includes 2 demagnetization fault modes (Mode 7D and Mode 8H), 22 electrical periods (1st~22nd), and 3 demagnetization severities (10%, 50%, 100%) as well as 2 operating conditions (rated speed and rated load, and 50% rated speed and 50% rated load). A total of 100 samples from each fault mode was randomly selected as training samples and the rest were test samples. Hence, the training database for the third PNN has 200 examples. The testing database for the second PNN has 108 examples, including 64 examples from the above 264 examples and 44 examples with different demagnetization severities from the training examples. A total of 44 examples ($2 \times 11 \times 2$) is composed of 22 examples for each fault mode including 11 electrical periods and 2 demagnetization severities (25% demagnetized (50% rated speed and rated load), and 75% demagnetized (rated speed and 50% rated load)).

3.4. Training Results

In this work, the PNN has been trained offline to learn the relationships between the DFISs (PNN inputs) and modes of demagnetization faults. The most important issue for the modeling of the PNN is the determination of an appropriate smoothing parameter σ, which is determined by SPREAD. First, we start by initializing SPREAD to 1; then, we change SPREAD until an appropriate value that provides us with a low training error is reached and no further improvement in classification can be obtained. In our mode, the

best training performances of the first PNN are obtained with SPREAD = 0.2, σ = 0.2. The second PNN is obtained with SPREAD = 0.1, σ = 0.1. The third PNN is obtained with SPREAD = 0.05, σ = 0.05;

The training outputs of the three PNNs are shown in Figure 12. The training accuracy is 99.5%, proving that the PNN has learned the input data well and has reproduced the desired outputs.

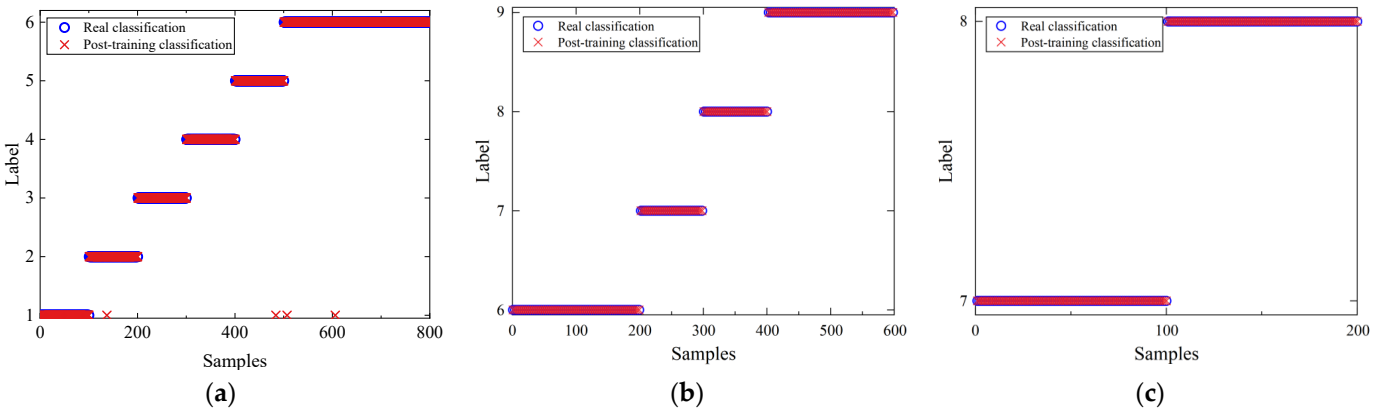


Figure 12. The training results of the three PNNs. (**a**) The first PNN. (**b**) The second PNN. (**c**) The third PNN.

3.5. Testing Results

The test procedure was made by the testing database, which is different from the training database, to assess the generalization capacity of the adopted PNNs.

The testing outputs of the three PNNs are shown in Figure 13. The training accuracy is 99%. This reveals the high accuracy and good generalization capacity of the developed PNN algorithm in identifying the modes of demagnetization faults.

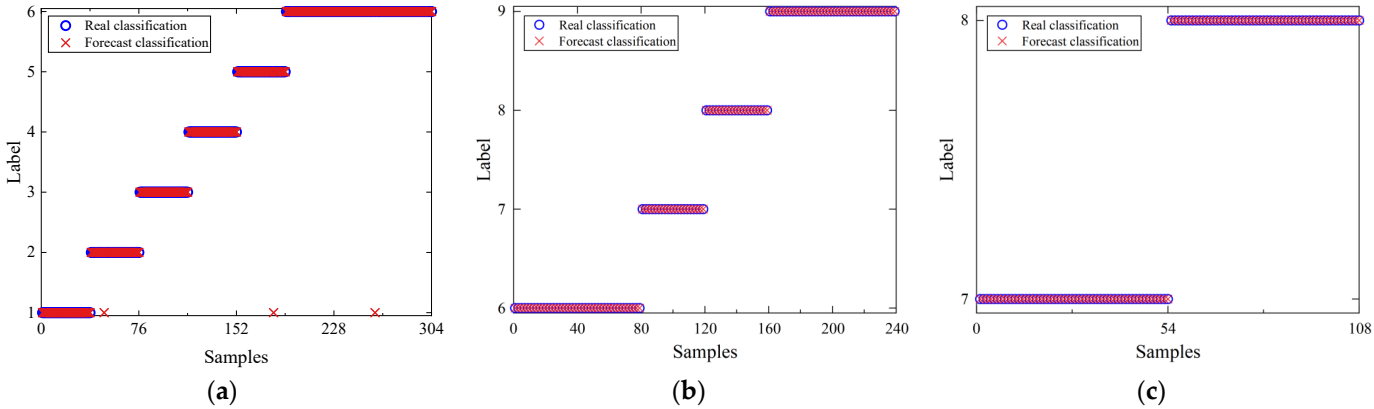


Figure 13. The testing results of the three PNNs. (**a**) The first PNN. (**b**) The second PNN. (**c**) The third PNN.

4. Simulation Results and Experimental Results

4.1. Simulation Results

To validate the effectiveness and superiority of the automatic demagnetization fault diagnosis method for DDPMSMs proposed in this paper, test data covering the different demagnetization faults and considering different operating conditions of the machine are required. For this purpose, the employed DDPMSM is modeled by FEM, which can collect data under healthy operating conditions and different operating conditions, and with different demagnetization fault modes with different operating conditions and different demagnetization fault parameters, since generally, those data are not available

for the real machine. Two healthy conditions and sixteen faulty modes are adopted (it is worth mentioning that the number, location, and severity of demagnetized PMs, and load and speed during testing are different from those for the training process). The healthy conditions are composed of different loads and different speeds (25% rated speed and 75% rated load, and 75% rated speed and 25% rated load). The faulty conditions are composed of two demagnetization faulty modes (PM1 demagnetization; PM2, PM43, and PM44 demagnetization), two demagnetization severities (5% and 15%), two load conditions (25% rated load and 75% rated load), and two speed conditions (50% rated speed and rated speed). The details of fault conditions and test results are listed in Table A4.

The simulation results in Table A4 show that the developed method can accurately determine the position of demagnetized permanent magnets under various operating conditions and different demagnetization fault parameters, indicating the high accuracy and strong robustness of the proposed demagnetization fault automatic diagnosis method based on three PNNs and toroidal-yoke-search coils.

It also can be seen from Table A4 that when the demagnetization severity is greater than 10%, the demagnetization fault can be detected and demagnetized permanent magnets can be located. The results indicate that the proposed demagnetization fault automatic diagnosis system can accurately diagnose demagnetization faults at the early stage. The results indicate that the method has high sensitivity.

4.2. Experimental Results

To validate the effectiveness of the automatic and accurate diagnosis method for demagnetization faults in DDPMSMs proposed in this paper, a prototype with demagnetization faults was developed, and a testing platform for fault characteristics of the machine was established, as shown in Figure 14.

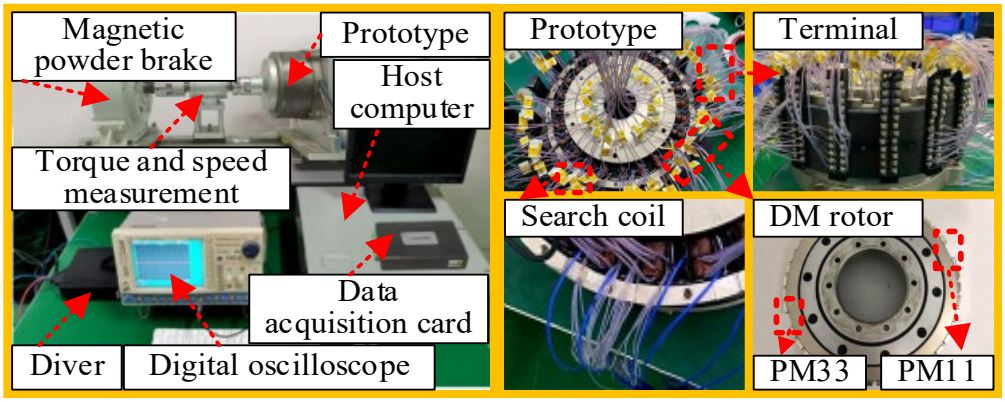


Figure 14. Experimental setup.

The experimental platform is composed of a prototype (Shenzhen, China, Yokokawa DMF280-270FE), a driver used to drive the prototype (Shenzhen, China, Yokokawa VCII-10-230), a magnetic powder brake (Haian, China, LanLing FZ400) a torque and speed measurement used to measure machine torque and speed (Beijing, China, BeiJingZhongHangKeDian ZH07-500Z), a DC power used to supply power to the magnetic powder brake (Haian, China, LanLing SC-1D), a host computer which is mainly responsible for data acquisition, storage, and fault diagnosis tasks (lenovo), a data acquisition card with 12 bit ADC resolutions used to collect the voltages of DFISs (American, NI USB-6009), and a digital oscilloscope (Shenzhen, China, Yokogawa 750). The implementation process of the experiment is as follows:

(1) Develop a healthy prototype installed with the toroidal-yoke-search coils proposed in this article. Specifications for the healthy prototype are the same as the machine described in Section 2.3, which are listed in Table 2. This healthy prototype is installed on the testing platform shown in Figure 14, and the voltages of three toroidal-yoke-search coils (TYC1, TYC2, and TYC3) are collected by NI USB-6009 and transmitted to a host computer through

USB connection. The voltages of TYC1 and TYC2 of the healthy prototype under rated load and rated speed are shown in Figure 15a, and the voltages of the SI_m of the healthy prototype under rated load and rated speed are shown in Figure 15b.

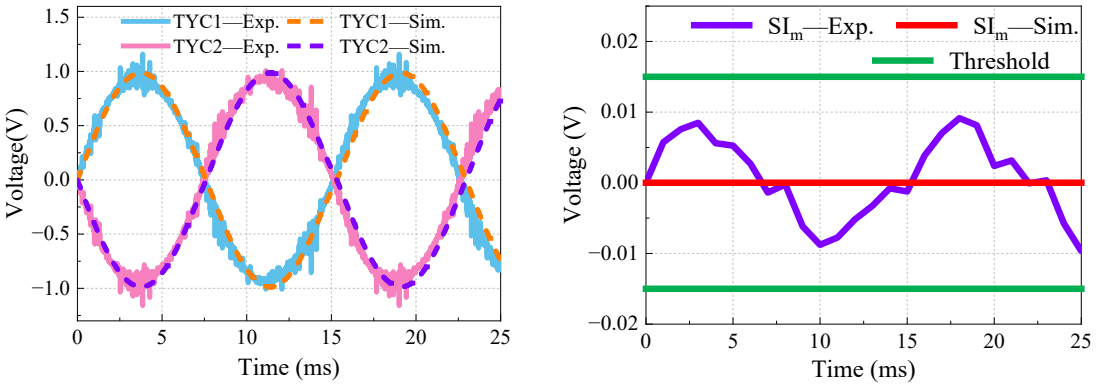


Figure 15. The experimental results of the voltage of TYC1, TYC2, and SI_m under healthy conditions. (**a**) The voltage waveform of TYC1 and TYC2. (**b**) The voltage waveform of SI_m.

(2) Develop a demagnetization faulty prototype installed with the toroidal-yoke-search coils proposed in this article. Specifications for the faulty prototype are the same as the machine described in Section 2.3, but two permanent magnets have been removed to simulate a demagnetization fault. In order to reduce the eccentricity caused by the removal of permanent magnets, two permanent magnets (PM 11 and PM33) symmetrical with respect to the rotor centerline were removed to simulate a fault with a 100% demagnetization of the two permanent magnets in prototype. This demagnetization faulty prototype is installed on the testing platform shown in Figure 14 too. The voltages of TYC1, TYC2, and TYC3 of the faulty prototype under rated load and rated speed are shown in Figure 16a, and the voltages of SI_m and SI_{a1} of the faulty prototype under rated load and rated speed are shown in Figure 16b.

(3) Partition SI_m, SI_{a1}, and SI_{a2} by electrical period, and input the partition signals to the three PNNs; then, the location of all demagnetized permanent magnets in the machine are identified.

Figure 15a depicts the voltages of TYC1 and TYC2 under healthy machine conditions for the experimental results and the simulation results. The simulation results of the voltages of TYC1 and TYC2 are highly similar to the experimental results; the maximum error of the two results is 2.4%. This is caused by unbalanced voltage caused by the inhomogeneity of the permanent magnet magnetic field, environmental noise, etc.

Figure 15b depicts the voltages of SI_m under healthy machine conditions for the experimental results and the simulation results. The simulation results of SI_m are in agreement with the experimental results; the maximum error of the two results is 1%. This is caused by environmental noise.

It can be observed from Figure 16a that the sixth and seventeenth electrical periods of the SI_m of the demagnetization faulty prototype (when PM11 and PM33 are removed) have a signal. Input the sixth and seventeenth electrical periods of the SI_m into the first PNN in sequence. The outputs of the first PNN are both six. Therefore, it is necessary to use the first auxiliary location signal S_{a1} for further classification.

It can be observed from Figure 16b that the sixth and seventeenth electrical periods of the SI_{a1} of demagnetization fault prototype have a signal. Input the sixth and seventeenth electrical periods of the SI_{a1} into the first PNN in sequence and input them into the second PNN in sequence. The outputs of the second PNN are both one. According to Table 3, the demagnetized PMs are PM1 and PM23.

The above simulation and experimental results validate the correctness and the effectiveness of the proposed automatic demagnetization fault diagnosis method based on three PNNs and toroidal-yoke-search coils for DDPMSMs.

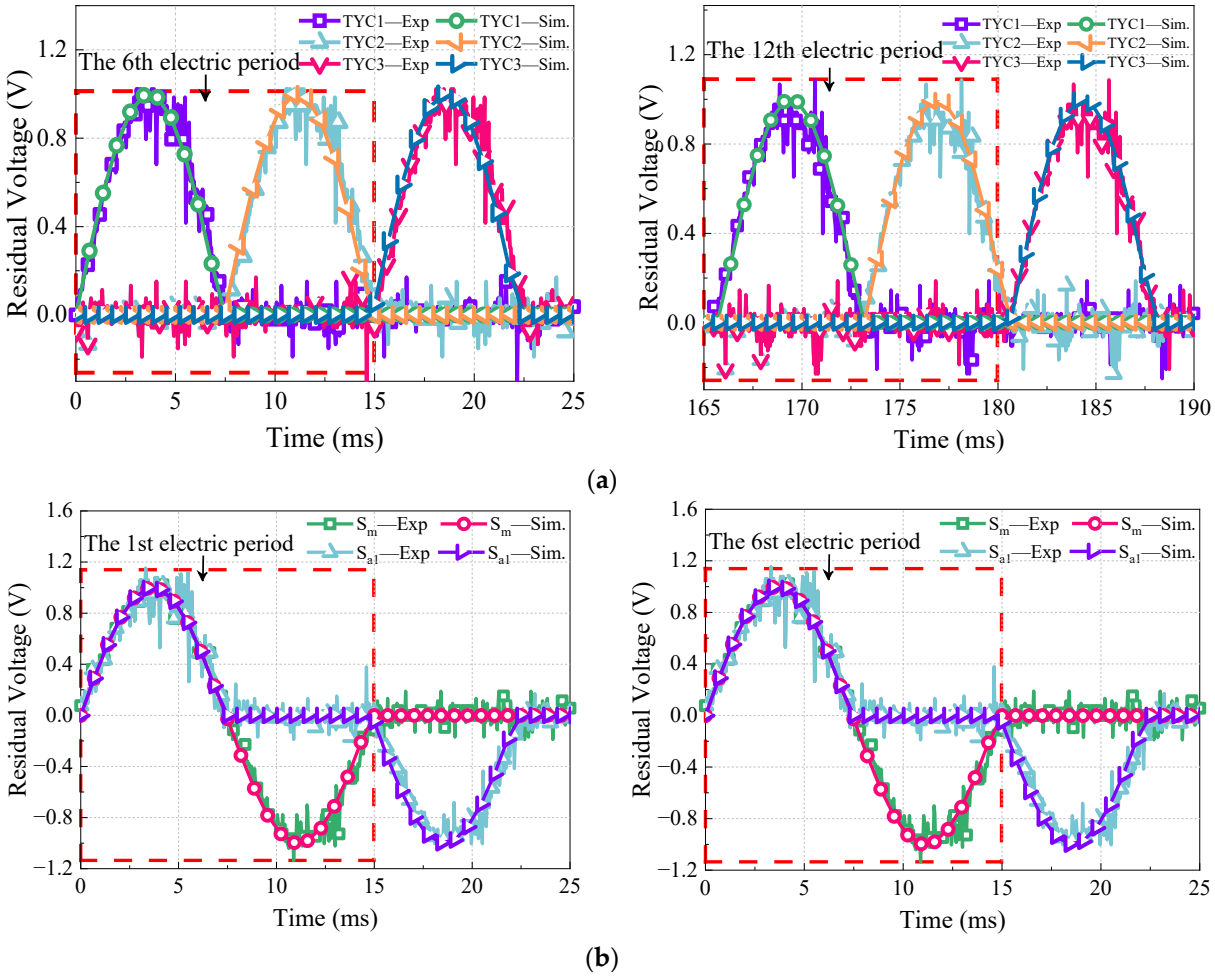


Figure 16. The experimental results of residual voltage of under fault3. (**a**) The residual voltage of TYC1, TYC2, and TYC3. (**b**) The residual voltage waveform of S_m and S_{a1}.

5. Conclusions

This paper proposes an automatic and accurate diagnosis method for demagnetization faults in PMSMs using three PNNs. The simulation and experimental results justify the correctness and effectiveness of the proposed method.

(1) Arranging three additional toroidal-yoke coils at the bottom of the three stator slots in DDPMSMs can capture many demagnetization faults, and not only contain early fault information, but also contain demagnetization fault location information. Compared with the existing search coil-based method, which installs a search coil on each tooth of the machine to locate the demagnetization faults, the number of search coils in this method is greatly reduced; therefore, it hardly increases the volume and cost of the machine, and does not disturb the design parameters and performance of the machine. Furthermore, the distance between adjacent toroidal-yoke coils is approximately polar distance. Thus, the design of the search coil does not need the structure parameters of the machine; it is easy to generalize this method to other PMSMs. In addition, the signal of toroidal-yoke coils is largely unaffected by magnetic circuit saturation, and therefore, the detection precision of the method is high.

(2) For PMSMs with very many magnetic poles, there are many modes of demagnetization faults, which makes it difficult to determine the number of demagnetized permanent

magnets. Therefore, this paper proposes a rotor partition method to solve this problem. The rotor permanent magnet is divided into zones according to each pair of permanent magnets, and the healthy condition of each pair of permanent magnets is diagnosed in turn, and then the demagnetized permanent magnets are located.

(3) Three demagnetization fault identified signals are constructed, which can indicate the location of demagnetized permanent magnets. Theoretical analysis and simulation results prove the robustness of the constructed signal to demagnetization degree, load, and speed.

(4) The three PNN-based diagnosis model is developed to determine demagnetization fault modes step by step. The constructed demagnetization fault identified signals are directly input into PNNs, and then the PNNs extract fault features and classify fault modes. Compared with the existing fault diagnosis methods based on deep learning, the proposed method realizes demagnetization fault mode classification with a lightweight model, and has the advantages of a simple network learning process and quick training. The accuracy and robustness of the developed diagnostics system using three PNNs were confirmed by testing unseen modes (captured experimentally and by FEM simulation). The overall accuracy of diagnosis is 99.2%.

Author Contributions: Conceptualization, Y.X. and K.W.; methodology, Y.X.; software, Y.X.; validation, J.Z. and Y.X.; formal analysis, S.Y. and K.W.; investigation, Y.X. and H.Z.; resources, S.Y.; data curation, S.Y.; writing—original draft preparation, Y.X. and K.W.; writing—review and editing, Y.X. and H.Z.; visualization, K.W.; supervision, Y.X. and H.Z.; project administration, Y.X.; funding acquisition, K.W. and J.Z. All authors have read and agreed to the published version of the manuscript.

Funding: This research was funded by a project supported by the National Natural Science Foundation of China: 51907201 and funding from the Military Logistics Research Program: BHJ22R047.

Institutional Review Board Statement: Not applicable.

Informed Consent Statement: Not applicable.

Data Availability Statement: The original contributions presented in the study are included in the article, further inquiries can be directed to the corresponding author.

Conflicts of Interest: The authors declare no conflict of interest.

Appendix A

Table A1. The first database for training and testing the first PNN.

#	Speed (rpm)	Current (Arms)	Fault Mode	Demagnetized PMs	Demagnetized Severity	(O)	T/F Diagnosis
1	200	28	Mode 1	/	/	1	T
⋮	⋮	⋮	⋮	⋮	⋮	⋮	T
132	100	14	Mode 1	/	/	1	T
133	200	28	Mode 2	PM2	10%	2	T
134	100	14	Mode 2	PM2	10%	2	T
135	200	28	Mode 2	PM2	50%	2	T
136	100	14	Mode 2	PM2	50%	2	T
137	200	28	Mode 2	PM2	100%	2	T
⋮	⋮	⋮	⋮	⋮	⋮	⋮	T
264	100	14	Mode 2	PM2	100%	2	T
265	200	28	Mode 3	PM44, PM1	10%	3	T
⋮	⋮	⋮	⋮	⋮	⋮	⋮	T
396	100	14	Mode 3	PM44, PM1	100%	3	T
397	200	28	Mode 4	PM1, PM2	10%	4	T
⋮	⋮	⋮	⋮	⋮	⋮	⋮	T

Table A1. *Cont.*

#	Speed (rpm)	Current (Arms)	Fault Mode	Demagnetized PMs	Demagnetized Severity	(O)	T/F Diagnosis
528	100	14	Mode 4	PM1, PM2	100%	4	T
529	200	28	Mode 5	PM44	10%	5	T
⋮	⋮	⋮	⋮	⋮	⋮	⋮	T
660	100	14	Mode 5	PM44	100%	5	T
661	200	28	Mode 6	PM1	10%	6	T
⋮	⋮	⋮	⋮	⋮	⋮	⋮	T
792	100	14	Mode 6	PM1	100%	6	T
793	200	28	Mode 7	PM44, PM2	10%	6	T
⋮	⋮	⋮	⋮	⋮	⋮	⋮	T
924	100	14	Mode 7	PM44, PM2	100%	6	T
925	200	28	Mode 8	PM44, PM1,PM2	10%	6	T
⋮	⋮	⋮	⋮	⋮	⋮	⋮	T
1056	100	14	Mode 8	PM44, PM1,PM2	100%	6	T

Table A2. The second database for training and testing the second PNN.

#	Speed (rpm)	Current (Arms)	Fault Mode	Demagnetized PMs	Demagnetized Severity	(O)	T/F Diagnosis
1	200	28	Mode 6H	PM1	10%	6	T
2	100	14	Mode 6H	PM1	10%	6	T
3	200	28	Mode 6H	PM1	30%	6	T
4	100	14	Mode 6H	PM1	30%	6	T
5	200	28	Mode 6H	PM1	50%	6	T
⋮	⋮	⋮	⋮	⋮	⋮	⋮	T
132	100	14	Mode 6H	PM1	50%	6	T
133	200	28	Mode 7H	PM44, PM2	10%	7	T
⋮	⋮	⋮	⋮	⋮	⋮	⋮	T
264	100	14	Mode 7H	PM44, PM2	50%	7	T
265	200	28	Mode 8H	PM44, PM1, PM2	10%	9	T
⋮	⋮	⋮	⋮	⋮	⋮	⋮	T
396	265	200	Mode 8H	PM44, PM1, PM2	50%	9	T
397	200	28	Mode 6D	PM43, PM1	10%	6	T
⋮	⋮	⋮	⋮	⋮	⋮	⋮	T
528	100	14	Mode 6D	PM43, PM1	50%	6	T
529	200	28	Mode 7D	PM43, PM44, PM2	10%	9	T
⋮	⋮	⋮	⋮	⋮	⋮	⋮	T
660	100	14	Mode 7D	PM43, PM44, PM2	50%	9	T
661	200	28	Mode 8D	PM43, PM44, PM1, PM2	10%	8	T
⋮	⋮	⋮	⋮	⋮	⋮	⋮	T
792	100	14	Mode 8D	PM43, PM44, PM1, PM2	50%	8	T
793	200	14	Mode 6H	PM1	75%	6	T
⋮	⋮	⋮	⋮	⋮	⋮	⋮	T
800	100	28	Mode 6H	PM1	25%	6	T
⋮	⋮	⋮	⋮	⋮	⋮	⋮	T
840	100	28	Mode 8D	PM43, PM44, PM1, PM2	25%	8	T

Table A3. The third database for training and testing the third PNN.

#	Speed (rpm)	Current (Arms)	Fault Mode	Demagnetized PMs	Demagnetized Severity	(O)	T/F Diagnosis
1	200	28	Mode 7D	PM43, PM44, PM2	10%	7	T
2	100	14	Mode 7D	PM43, PM44, PM2	10%	7	T
3	200	28	Mode 7D	PM43, PM44, PM2	50%	7	T
4	100	14	Mode 7D	PM43, PM44, PM2	50%	7	T
5	200	28	Mode 7D	PM43, PM44, PM2	100%	7	T
⋮	⋮	⋮	⋮	⋮	⋮	⋮	T
132	100	14	Mode 7D	PM43, PM44, PM2	100%	7	T
133	200	28	Mode 8H	PM44, PM1, PM2	10%	8	T
⋮	⋮	⋮	⋮	⋮	⋮	⋮	T
264	100	14	Mode 8H	PM44, PM1, PM2	100%	8	T
265	200	14	Mode 7D	PM43, PM44, PM2	75%	7	T
⋮	⋮	⋮	⋮	⋮	⋮	⋮	T
286	100	28	Mode 7D	PM43, PM44, PM2	25%	7	T
287	200	14	Mode 8H	PM44, PM1, PM2	75%	8	T
⋮	⋮	⋮	⋮	⋮	⋮	⋮	T
308	100	28	Mode 8H	PM44, PM1, PM2	25%	8	T

Table A4. The details of fault conditions and test results.

Fault Number	Setting Demagnetization PM Number	Signal Used	Electrical Period Number	Identified Fault Type	Identified Demagnetization PM Number
fault1	PM20	SI_{m}	10th	Mode 3	PM20
		SI_{m}	11th	Mode 5	PM20
fault2	PM43,44,2	SI_{m}	1st	Mode 2/7/8	
		SI_{a1}	1st	Mode 7B/8A	
		SI_{a2}	1st	Mode 7B	PM43,44,2
		SI_{m}	2nd	Mode 5	PM2
		SI_{m}	22th	Mode 4	PM43,44

References

1. Candelo-Zuluaga, C.; Riba, J.-R.; Espinosa, A.G.; Blanch, P.T. Customized PMSM Design and Optimization Methodology For Water Pumping Applications. *IEEE Trans. Energy Convers.* **2022**, *37*, 454–465. [CrossRef]
2. Fang, S.; Liu, H.; Wang, H.; Yang, H.; Lin, H. High Power Density PMSM With Lightweight Structure and High-Performance Soft Magnetic Alloy Core. *IEEE Trans. Appl. Supercond.* **2019**, *29*, 0602805. [CrossRef]
3. Xie, J.; Zhang, X.; Guo, J.; Qin, G.; Huang, F.; Huang, S.; Long, Z. Fault Detection of Permanent Magnet Synchronous Motor Based on Image Content Retrieval. *IEEE Trans. Instrum. Meas.* **2022**, *71*, 3530010. [CrossRef]
4. Huang, F.; Zhang, X.; Qin, G.; Xie, J.; Peng, J.; Huang, S.; Long, Z.; Tang, Y. Demagnetization Fault Diagnosis of Permanent Magnet Synchronous Motors Using Magnetic Leakage Signals. *IEEE Trans. Ind. Inform.* **2023**, *19*, 6105–6116. [CrossRef]
5. Zhao, K.; He, J.; Huang, G.; Li, X. Demagnetization-Fault Reconstruction and Tolerant-Control for PMSM Using Improved SMO-Based Equivalent-Input-Disturbance Approach. *IEEE-ASME Trans. Mech.* **2022**, *27*, 701–712. [CrossRef]
6. Kuruppu, S.S.; Abeyratne, S.G. Disambiguation of Uniform Demagnetization Fault From Position Sensor Fault in FOC PMSM Applications. *IEEE Access* **2022**, *10*, 103099–103110. [CrossRef]
7. Ruiz, J.-R.R.; Rosero, J.A.; Espinosa, A.G.; Romeral, L. Detection of Demagnetization Faults in Permanent-Magnet Synchronous Motors Under Nonstationary Conditions. *IEEE Trans. Magn.* **2009**, *45*, 2961–2969. [CrossRef]
8. Urresty, J.-C.; Riba, J.-R.; Romeral, L. Influence of the Stator Windings Configuration in the Currents and Zero-Sequence Voltage Harmonics in Permanent Magnet Synchronous Motors With Demagnetization Faults. *IEEE Trans. Magn.* **2013**, *49*, 4885–4893. [CrossRef]
9. Rosero, J.A.; Cusido, J.; Garcia, A.; Ortega, J.A.; Romeral, L. Study on the Permanent Magnet Demagnetization Fault in Permanent Magnet Synchronous Machines. In Proceedings of the IECON 2006—32nd Annual Conference on IEEE Industrial Electronics, Paris, France, 7–10 November 2006; pp. 879–884.

10. Torregrossa, D.; Khoobroo, A.; Fahimi, B. Prediction of Acoustic Noise and Torque Pulsation in PM Synchronous Machines with Static Eccentricity and Partial Demagnetization Using Field Reconstruction Method. *IEEE Trans. Ind. Electron.* **2012**, *59*, 934–944. [CrossRef]
11. Goktas, T.; Zafarani, M.; Lee, K.W.; Akin, B.; Sculley, T. Comprehensive Analysis of Magnet Defect Fault Monitoring Through Leakage Flux. *IEEE Trans. Magn.* **2017**, *53*, 8201010. [CrossRef]
12. Cheng, M.; Hang, J.; Zhang, J. Overview of Fault Diagnosis Theory and Method for Permanent Magnet Machine. *Chin. J. Electr. Eng.* **2015**, *1*, 21–36. [CrossRef]
13. Chen, H.; Gao, C.; Si, J.; Nie, Y.; Hu, Y. A Novel Method for Diagnosing Demagnetization Fault in PMSM Using Toroidal-Yoke-Type Search Coil. *IEEE Trans. Instrum. Meas.* **2022**, *71*, 7501012. [CrossRef]
14. Rafaq, M.S.; Lee, H.-J.; Park, Y.; Lee, S.B.; Zapico, M.O.; Fernandez, D.; Reigosa, D. Airgap Search Coil Based Identification of PM Synchronous Motor Defects. *IEEE Trans. Ind. Electron.* **2022**, *69*, 6551–6560. [CrossRef]
15. Zeng, C.; Huang, S.; Lei, J.; Wan, Z.; Yang, Y. Online Rotor Fault Diagnosis of Permanent Magnet Synchronous Motors Based on Stator Tooth Flux. *IEEE Trans. Ind. Appl.* **2021**, *57*, 2366–2377. [CrossRef]
16. Da, Y.; Shi, X.; Krishnamurthy, M. A New Approach to Fault Diagnostics for Permanent Magnet Synchronous Machines Using Electromagnetic Signature Analysis. *IEEE Trans. Power Electron.* **2013**, *28*, 4104–4112. [CrossRef]
17. Singh, M.; Shaik, A.G. Incipient Fault Detection in Stator Windings of an Induction Motor Using Stockwell Transform and SVM. *IEEE Trans. Instrum. Meas.* **2020**, *69*, 9496–9504. [CrossRef]
18. Liang, Y.; Li, K.-J.; Ma, Z.; Lee, W.-J. Multilabel Classification Model for Type Recognition of Single-Phase-to-Ground Fault Based on KNN-Bayesian Method. *IEEE Trans. Ind. Appl.* **2021**, *57*, 1294–1302. [CrossRef]
19. Nyanteh, Y.; Srivastava, S. Application of Artificial Intelligence to Real-Time Fault Detection in Permanent-Magnet Synchronous Machines. *IEEE Trans. Ind. Appl.* **2013**, *49*, 1205–1214. [CrossRef]
20. Bouzid, M.B.K.; Champenois, G. An Efficient Simplified Physical Faulty Model of a Permanent Magnet Synchronous Generator Dedicated to Stator Fault Diagnosis Part II: Automatic Stator Fault Diagnosis. *IEEE Trans. Ind. Appl.* **2017**, *53*, 2762–2771. [CrossRef]
21. Maraaba, L.S.; Al-Hamouz, Z.M.; Milhem, A.S.; Abido, M.A. Neural Network-Based Diagnostic Tool for Detecting Stator Inter-Turn Faults in Line Start Permanent Magnet Synchronous Motors. *IEEE Access* **2019**, *7*, 89014–89025. [CrossRef]
22. Zhang, J.; Zhang, D.; Shen, G.; Yang, J. Research on Fault Diagnosis of Marine Diesel Engine Based on Probabilistic Neural Network Optimized by Quantum Genetic Algorithm. In Proceedings of the 2021 IEEE 4th International Conference on Automation, Electronics and Electrical Engineering (AUTEEE), Shenyang, China, 19–21 November 2021; pp. 729–733.
23. Liu, F.; Gao, J.; Liu, H. The Feature Extraction and Diagnosis of Rolling Bearing Based on CEEMD and LDWPSO-PNN. *IEEE Access* **2020**, *8*, 19810–19819. [CrossRef]

Disclaimer/Publisher's Note: The statements, opinions and data contained in all publications are solely those of the individual author(s) and contributor(s) and not of MDPI and/or the editor(s). MDPI and/or the editor(s) disclaim responsibility for any injury to people or property resulting from any ideas, methods, instructions or products referred to in the content.